

Rabi and Ramsey oscillations of a Majorana qubit in a quantum dot-superconductor array

Haining Pan,¹ Sankar Das Sarma,² and Chun-Xiao Liu^{3,*}

¹*Department of Physics and Astronomy, Center for Materials Theory, Rutgers University, Piscataway, NJ 08854 USA*

²*Condensed Matter Theory Center and Joint Quantum Institute,*

Department of Physics, University of Maryland, College Park, Maryland 20742, USA

³*QuTech and Kavli Institute of NanoScience, Delft University of Technology, Delft, The Netherlands*

(Dated: July 25, 2024)

The Kitaev chain can be engineered within a quantum dot-superconductor array, hosting Majorana zero modes at fine-tuned sweet spots. In this work, we propose and simulate the occurrence of Rabi and Ramsey oscillations to feasibly construct a minimal Majorana qubit in the quantum dot setup. Our real-time results incorporate realistic effects, e.g., charge noise and leakage, reflecting the latest experimental progress. We demonstrate that Majorana qubits with larger energy gaps exhibit significantly enhanced performance—longer dephasing times, higher quality factors, reduced leakage probabilities, and improved visibilities—compared to those with smaller gaps and with conventional quantum dot-based charge qubits. We introduce a method for reading out Majorana qubits via quantum capacitance measurements. Our work paves the way for future experiments on realizing Majorana qubits in quantum dot-superconductor arrays.

Introduction.—Majorana zero modes are non-Abelian anyonic excitations localized at the defects or edges of a topological superconductor [1–16]. Qubits constructed from the Majorana excitations are immune to local noise and are fault-tolerant without active error corrections, offering a pathway to implementing error-resilient topological quantum computing [3, 9]. Recently the quantum dot-superconductor array has become a promising candidate for realizing topological Kitaev chains [2] in solid-state physics using a concrete idea proposed a while ago [17]. An advantage of this quantum-dot-based approach is the intrinsic robustness against the effect of disorder that is ubiquitous in semiconductor-superconductor Majorana platforms [18–22]. In addition, utilizing Andreev bound states in a hybrid region as coupler enables precise control over the relative amplitudes of normal and superconducting interactions between quantum dots [23–27], thus allowing for fine-tuning of a quantum dot-superconductor array into a sweet spot with optimally protected Majorana zero modes [2, 17, 28]. Tunnel spectroscopic signatures of Majoranas have been observed in recent experiments on quantum dots using both nanowires [29–31] and two-dimensional electrons [32].

To decisively establish a Majorana qubit and demonstrate its topologically enhanced coherence, Rabi oscillation experiments on quantum-dot-based Kitaev chains are necessary [33]. Additionally, understanding the topological coherence and obtaining a sufficiently long coherence time is crucial for detecting the non-Abelian statistics of Majorana anyons in fusion [34] or braiding experiments [35, 36]. Most importantly (and we demonstrate in the current work), such a Rabi oscillation experiment is already feasible in currently available platforms [29–32], provided that two such minimal Kitaev chains are interconnected via a common superconducting lead, and

normal-tunnel-coupled at their ends [see Fig. 1(a)].

In the current work, we propose Rabi and Ramsey oscillation experiments in a minimal Majorana qubit composed of double two-site Kitaev chains [see Fig. 1(a)]. Our real-time simulations incorporate realistic effects such as charge noise and leakage to the non-computational bases. We find that Majorana qubits constructed from large-gap Kitaev chains significantly outperform those with smaller gaps and conventional quantum dot-based charge qubits in terms of dephasing time, quality factor, leakage probability, and visibility. In addition, we propose a Majorana qubit readout method based on quantum capacitance. Our work demonstrates the optimal route to the first step of establishing Majorana qubit as a viable experimental entity, which has not been achieved in the fifteen years of experiments [37–40] and twenty-five years of theory [1–3, 41–43] on topological quantum computing.

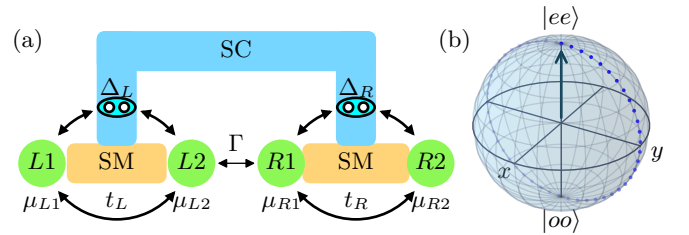


FIG. 1. (a) Schematic of a Majorana qubit composed of double two-site Kitaev chains. (b) Bloch sphere. $|\pm z\rangle$ are defined as $|ee\rangle$ and $|oo\rangle$, respectively. The dots represent the trajectory of the state vector in a Rabi experiment.

Setup and Hamiltonian.—A minimal Majorana qubit consists of double two-site Kitaev chains, as shown in

Fig. 1(a). The Hamiltonian is

$$\begin{aligned}\mathcal{H}_{\text{tot}} &= \mathcal{H}_L + \mathcal{H}_R + \mathcal{H}_{\text{tunn}}, \\ \mathcal{H}_a &= \sum_{i=1}^2 \mu_{ai} n_{ai} + \left(t_a c_{a2}^\dagger c_{a1} + \Delta_a c_{a2} c_{a1} + \text{H.c.} \right), \\ \mathcal{H}_{\text{tunn}} &= \Gamma c_{R1}^\dagger c_{L2} + \text{H.c.}\end{aligned}\quad (1)$$

Here \mathcal{H}_a with $a \in \{L, R\}$ is the Hamiltonian for the left and right chain, respectively, with μ_{ai} ($i = 1, 2$) the onsite energy of a spin-polarized dot orbital, $n_{ai} = c_{ai}^\dagger c_{ai} = 0, 1$ the occupancy number, and t_a and Δ_a the strengths of the normal and Andreev tunnelings. $\mathcal{H}_{\text{tunn}}$ is the tunnel Hamiltonian, with Γ being the strength of single-electron transfer between dots from different chains. In the current work, we are particularly interested in the sweet spot of the system, which is defined as $\mu_{ai} = 0$ and $t_a = \Delta_a$. At that point, the even-parity ground state $|e\rangle_a = (|00\rangle_a - |11\rangle_a)/\sqrt{2}$ is degenerate with the odd-parity one $|o\rangle_a = (|10\rangle_a - |01\rangle_a)/\sqrt{2}$ within each Kitaev chain, hosting a pair of Majorana zero modes at two separate quantum dots. Here $|n_1 n_2\rangle_a = \left(c_{a1}^\dagger\right)^{n_1} \left(c_{a2}^\dagger\right)^{n_2} |0\rangle_a$, and $|0\rangle_a$ is the vacuum state of chain- a . Since total Fermion parity is conserved in the Hamiltonian of Eq. (1), we can focus on the subspace with total parity even without loss of generality. As such, the ground-state degeneracy is two-fold:

$$|ee\rangle \equiv |e\rangle_L \otimes |e\rangle_R, \quad |oo\rangle \equiv |o\rangle_L \otimes |o\rangle_R, \quad (2)$$

which form the basis states of a Majorana qubit.

Rabi oscillations.—In the qubit subspace spanned by $|ee\rangle$ and $|oo\rangle$, the low-energy effective Hamiltonian is

$$H_{\text{eff}} = \frac{\varepsilon}{2} \sigma_z + \frac{\Gamma}{2} \sigma_x, \quad (3)$$

where $\varepsilon \equiv E_{oo} - E_{ee}$ and $\sigma_{x/z}$ are Pauli X/Z matrices. Here σ_z rotation is proportional to the ground-state energy splitting, which we choose to be $\varepsilon = t_L - \Delta_L$ by detuning the hybrid region in the left chain [30]. σ_x rotation is realized by single electron tunneling between the two chains that can be controlled by a tunnel barrier. Motivated by the form of H_{eff} in Eq. (3), we perform a numerical simulation of the Rabi and Ramsey experiments using the total Hamiltonian \mathcal{H}_{tot} in Eq. (1). Here we implement the qubit rotations by applying sequences of pulses of ε or Γ instead of microwave driving because of the basis state degeneracy. In particular, in the Rabi experiment the system is initialized in $|ee\rangle$ of two decoupled Kitaev chains at their sweet spots. This corresponds to the north pole of the Bloch sphere. We then turn on the inter-chain tunneling Γ and let the system evolve for a time τ before performing a readout in the σ_z basis [see pulse profiles in Fig. 2(a)]. Figure 2(b) shows the numerically calculated $P_{ee}(\tau) \equiv |\langle ee | \psi(\tau) \rangle|^2$

in the (Γ, τ) plane. Indeed, the fringe pattern of Rabi oscillations confirms that single-electron tunneling H_{tunn} in Eq. (1) works as a σ_x rotation in the qubit subspace, with the oscillation frequency being proportional to Γ . However, surprisingly, we also find that the state wavefunction can leak out of the qubit subspace with a probability $P_{\text{leak}}(\tau) \equiv 1 - P_{ee}(\tau) - P_{oo}(\tau)$, which oscillates periodically in time and increases with the tunneling strength Γ [see Fig. 2(c)]. Using time-dependent perturbation theory [44], we show that a finite inter-chain tunneling Γ inevitably induces a leakage to the excited states of $|e'e'\rangle$ and $|o'o'\rangle$, i.e.

$$P_{\text{leak}}(\tau) = P_{e'e'}(\tau) + P_{o'o'}(\tau) \approx \frac{\Gamma^2}{16\Delta^2} \sin^2(2\Delta\tau/\hbar), \quad (4)$$

where $|e'\rangle_a = (|00\rangle_a + |11\rangle_a)/\sqrt{2}$ and $|o'\rangle_a = (|10\rangle_a + |01\rangle_a)/\sqrt{2}$ are excited states in each chain and $\Delta_L = \Delta_R = \Delta$. Here the oscillation frequency of the leakage probability is $4\Delta/\hbar$ and the magnitude scales with Γ^2/Δ^2 . On the other hand, in a Ramsey experiment we first apply a pulse of H_{tunn} to rotate the initial state $|ee\rangle$ to the equator of the Bloch sphere, then let it evolve for a time duration τ_{wait} in the presence of a finite ε , and apply the same H_{tunn} pulse again before the final readout [see pulse profiles in Fig. 2(d)]. The simulated $P_{ee}(\tau)$ in the $(\varepsilon, \tau_{\text{wait}})$ plane is shown in Fig. 2(e). Here the small P_{leak} in Fig. 2(f) is due to the σ_x pulses, while detuning the coupling $t_L - \Delta_L$ has a negligible impact on the leakage probability. Both experiments are doable in the currently available devices and provide complementary information about Majorana coherence.

Qubit dephasing.—Charge noise is one of the primary sources of decoherence in semiconductor-based qubits [45–52]. It can be induced by charge impurities in the environment or fluctuations in the gate voltages nearby. As a $1/f$ noise, the fluctuations are dominated by the low-frequency components, which can be modeled by the quasi-static disorder approximation, since the zero-frequency part of the noise dominates [53, 54]. That is, in each run of the Rabi or Ramsey experiment the Hamiltonian parameters in Eq. (1) are subject to a static disorder that obeys normal distribution, and the final readout measurement is averaged over 500 different disorder realizations, giving $\langle P_{ee}(\tau) \rangle$. In particular, we simulate and compare three different types of qubits: 1) semiconductor charge qubit with one electron in double quantum dots [52, 55], 2) small-gap Majorana qubit [29], and 3) large-gap Majorana qubit [30, 32]. Here a small (large) gap in the Kitaev chain corresponds to the scenario where the dot-hybrid coupling strength is smaller than (comparable to) the induced gap in the hybrid region [56]. The mean values and standard deviations of Hamiltonian parameters that are subject to charge noises are chosen according to the values reported in relevant

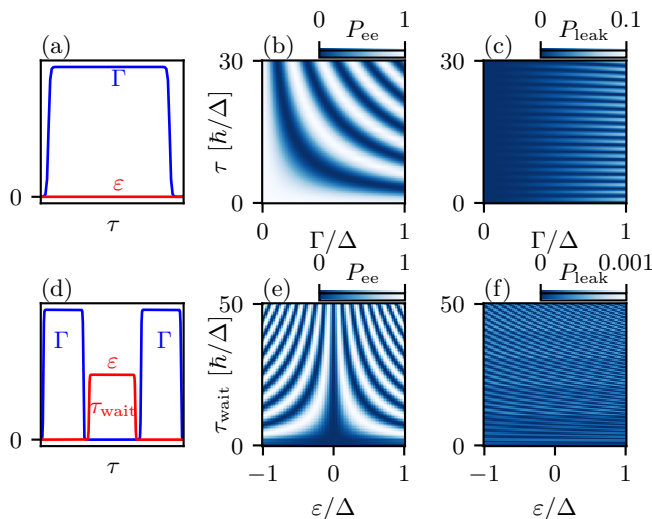


FIG. 2. Numerical simulations in the clean limit. Upper panels: Numerical simulation of a Rabi experiment. (a) Pulse profiles. (b) and (c) P_{ee} and P_{leak} in Eq. (4) in the (Γ, τ) plane. Lower panels: Numerical simulation of a Ramsey experiment. (d) Pulse profiles. (e) and (f) P_{ee} and P_{leak} in the $(\varepsilon, \tau_{wait})$ plane. Here $\Delta_L = \Delta_R = \Delta$.

experimental works, which are summarized in the supplemental materials [44]. Figure 3 shows the calculated Rabi and Ramsey oscillations of $\langle P_{ee}(\tau) \rangle$ with dephasing for all three types of qubits. The curves with decaying envelopes are further fitted using the following formula

$$\langle P_{ee}(\tau) \rangle = P_0 + A \cos(2\pi f\tau + \phi_0) \exp\{-(\tau/T_2)^\beta\}, \quad (5)$$

where $2A$ is the visibility, T_2 is the dephasing time, and β is the decaying exponent. Their values are summarized in Table I, and in addition we define the quality factor as $Q = 2\pi fT_2$ and the leakage probability as $P_{leak} = \lim_{\tau_0 \rightarrow \infty} \int_0^{\tau_0} \langle P_{leak}(\tau) \rangle d\tau / \tau_0$ in the long time limit where $\langle P_{leak}(\tau) \rangle = 1 - \langle P_{ee}(\tau) \rangle - \langle P_{oo}(\tau) \rangle$ is the instantaneous value.

The Hamiltonian for a semiconductor charge qubit is

$$H_c = \begin{pmatrix} \varepsilon_L & \Gamma \\ \Gamma & \varepsilon_R \end{pmatrix}, \quad (6)$$

where the basis states are $|10\rangle$ and $|01\rangle$ with one electron in the left or right quantum dot, ε_L (ε_R) is the corresponding orbital energy in the left (right) dot, and Γ is the interdot coupling strength. Here, the fluctuations of the dot energies σ_ε dominate the dephasing effect, compared to the fluctuations of the interdot coupling strength σ_Γ , due to the small magnitude of Γ . In the Rabi experiment, the dot energies are tuned into a sweet spot of $\varepsilon_L = \varepsilon_R = 0$, which is insensitive to dot-energy detuning up to the first order, i.e., $\partial E / \partial \varepsilon_a = 0$. However, since the dot-energy fluctuations are large and comparable to the interdot coupling strength, e.g., $\sigma_\varepsilon = 3 \mu\text{eV} \simeq \Gamma = 5 \mu\text{eV}$, the higher-order

contributions (e.g., $\delta E \sim \sigma_\varepsilon^2 / \Gamma$) lead to a short dephasing time $T_2 \approx 2.50(7)$ ns for x rotations, see Fig. 3(a). In the Ramsey experiment, to implement the z rotation, we choose $\varepsilon_L = -\varepsilon_R = 20 \mu\text{eV} \gg \Gamma$, which is much more susceptible to charge noise as $\partial E / \partial \varepsilon_a \approx 1$. Thus, the dephasing time is even shorter $T_2 \approx 0.096(2)$ ns and the visibility is reduced, see Fig. 3(d). The consistency between our T_2 estimates and the experimental measurements reported in Ref. [55] validates our modeling of the quantum dot devices.

In a minimal two-site Kitaev chain that is in the vicinity of the sweet spot, the energy splitting between the even- and odd-parity ground states is approximately $E \equiv E_o - E_e \approx \mu_1 \mu_2 / 2t + (t - \Delta)$, where the first term is due to the simultaneous detuning of onsite dot energies, while the second term is the detuning of the hybrid region. In a small-gap Majorana qubit (i.e., small $t \equiv \Delta$ limit), the dot-energy fluctuations are comparatively dominant, giving a characteristic energy splitting between the basis states $\delta E \sim \sigma_\mu^2 / t$. For a Majorana qubit defined in Fig. 1(a), such a δE leads to noises in the σ_z basis. In the Rabi experiment, since the dot-energy noise ($\propto \sigma_z$) is orthogonal to the σ_x rotation, the dephasing effect of the dot energy fluctuations is strongly mitigated [44]. As such, $T_2 \approx 9.25(5)$ ns is jointly determined by the fluctuations in the dot energies ($\propto \sigma_z$) as well as in the interchain coupling strengths ($\propto \sigma_x$), see Fig. 3(b). In the Ramsey experiment on σ_z rotations, the large dot-energy fluctuations ($\propto \sigma_z$) cause a more detrimental effect on qubit dephasing, giving a much shorter dephasing time $T_2 \approx 1.84(7)$ ns and a reduced visibility $2A \approx 0.3716(8)$, see Fig. 3(e) and Table I. Note that here the dephasing effect of charge noise in t_a and Δ_a is negligible because of the weak dot-superconductor hybridization.

On the contrary, the performance of a large-gap Majorana qubit is much improved in almost all aspects, e.g., dephasing time, quality factor, visibility, and leakage probability. The strong dot-superconductor hybridization not only strongly enhances the excitation gap of a Kitaev chain, but also transforms the dot orbitals into Yu-Shiba-Rusinov states [57–59], thus significantly screening the electric charge in the quantum dots [30, 32, 56]. As a result, the energy splitting due to μ_{ai} fluctuations in the effective Kitaev chain is strongly suppressed, i.e., σ_μ^2 / t is reduced by a factor of ~ 300 compared to the small-gap Majorana qubit. Now the dominant source of dephasing in the Rabi experiment is the charge noise in Γ , giving $T_2 \approx 19.064(8)$ ns, see Fig. 3(c). In the Ramsey experiment, the fluctuations of $t_a - \Delta_a$ begin to dominate the dephasing, giving $T_2 \approx 11.23(1)$ ns, see Fig. 3(f). In addition, a larger excitation gap in the Majorana qubit also greatly suppresses the leakage probabilities (see Table I), consistent with the analytic estimates shown in Eq. (4).

Qubit readout.—To read out the Majorana qubits, we

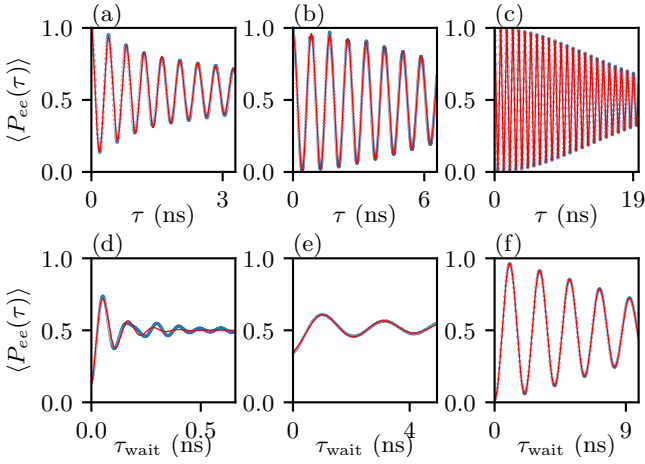


FIG. 3. Numerical simulations including charge noises. Upper panels: Rabi oscillations of disorder-averaged $\langle P_{ee} \rangle$. Lower panels: Ramsey oscillations of disorder-averaged $\langle P_{ee} \rangle$. (a) and (d) semiconductor charge qubits. (b) and (e) small-gap Majorana qubits. (c) and (f) large-gap Majorana qubits. The blue dots are data from numerical simulations, while the red lines are fitting curves using Eq. (5). Here, the size of the disorder ensemble is 500.

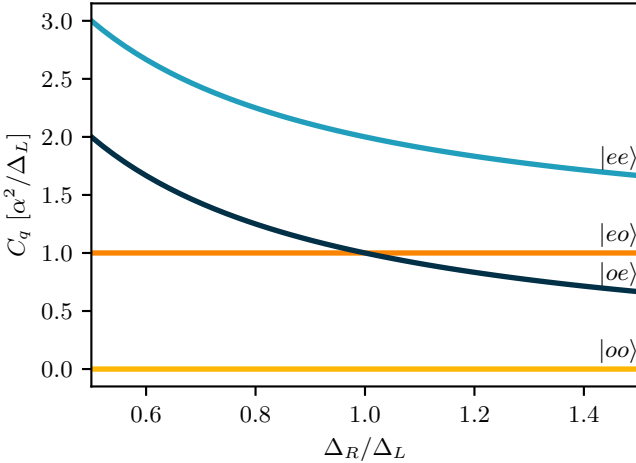


FIG. 4. Quantum capacitance readout in Eq. (7) of the low-energy states in a Majorana qubit. α is the magnitude of the lever arm of quantum dots, assumed to be identical for all dots. Δ_L (Δ_R) are the superconducting coupling strengths in the left (right) chains.

consider quantum capacitance measurement, which is defined as

$$C_q = -\frac{\partial^2 E}{\partial V_g^2} \quad (7)$$

in the zero-temperature limit [34]. Here E is the eigenenergy, V_g is the gate voltage that controls the dot energy via $\mu_{ai} = \alpha_{ai} V_g$ with α_{ai} being the lever arm. Since the measurement is performed when the two chains are decoupled, the result would simply be a sum of the values

TABLE I. Comparison of qubit performances.

Protocol	Qubit properties	Charge qubit	Small-gap Majorana qubit	Large-gap Majorana qubit
Rabi	T_2 (ns)	2.50(7)	9.25(5)	19.064(8)
	Q	38(1)	69.4(4)	144.7(5)
	$2A$	1.01(2)	0.958(1)	1.001(3)
	P_{leak}	-	0.035	$5.7(8) \times 10^{-4}$
	β	0.66(2)	1.87(2)	1.941(3)
Ramsey	T_2 (ns)	0.096(2)	1.84(7)	11.23(1)
	Q	5.3(2)	5.6(2)	34.31(3)
	$2A$	0.77(2)	0.3716(8)	0.950(5)
	P_{leak}	-	0.0275(1)	$3.31(6) \times 10^{-5}$
	β	1.01(4)	0.57(2)	1.557(4)

in each chain, i.e., $C_q = C_{qL} + C_{qR}$. Furthermore, in the equal-lever-arm regime ($\alpha_{a1} = \alpha_{a2} \equiv \alpha$), the quantum capacitance comes only from the even-parity state within each chain, while that of the odd-parity one is strongly suppressed [34]. Thus the quantum capacitances of $|ee\rangle$ and $|oo\rangle$ are

$$C_q^{ee} = \frac{\alpha^2}{\Delta_L} + \frac{\alpha^2}{\Delta_R}, \quad C_q^{oo} = 0, \quad (8)$$

which are distinct from each other and therefore can be used for qubit readout [44]. Following the argument, we further obtain that $C_q^{eo} = \alpha^2/\Delta_L$ and $C_q^{oe} = \alpha^2/\Delta_R$, which are different from both C_q^{ee} and C_q^{oo} . Therefore in addition to qubit readout, C_q measurement can simultaneously reveal the quasiparticle poisoning effect that transitions a Majorana qubit between states in different parity space.

Discussion.—In the numerical simulations, we regard $1/f$ charge noise as the dominant source of decoherence in the proposed devices, neglecting the quasiparticle poisoning effect because this is the prevailing situation in semiconductor platforms. For example, a poisoning time around ~ 1 ms, as reported in a similar semiconductor-superconductor hybrid device [60], is much longer than the dephasing time considered here ~ 10 ns, making poisoning insignificant for the current consideration where $1/f$ charge noise dominates decoherence. In addition, here both Rabi and Ramsey experiments are simulated using the most basic protocols for x and z rotations in order to demonstrate the working principles and to provide a fair comparison between semiconductor charge qubits and Majorana qubits. We emphasize that the system we consider [29–32] is equivalent to semiconductor charge qubits if all superconductivity is removed from considerations. It is, therefore, possible to further improve the dephasing time, e.g., by optimizing the pulse profiles, by designing a form of interdot coupling that is more resilient against charge noises, or by further scaling up the Kitaev chain [27, 31, 61]. Such considerations should be relevant once the basic Rabi and Ramsey oscillations pro-

posed by us are observed so that the elementary concept of a Majorana qubit is established beyond the simplest transport measurements prevalent so far in this subject. We emphasize that our work establishes the feasibility of Rabi oscillations in the already existing experimental platforms of Refs. [29–32].

Summary.—We propose and simulate Rabi and Ramsey oscillation experiments for a minimal Majorana qubit defined in coupled quantum dot-superconductor arrays. Our realistic calculations demonstrate that the performance of large-gap Majorana qubits significantly surpasses that of small-gap counterparts and traditional conventional charge qubits, although some enhancement over semiconductor charge qubits should already manifest in the small-gap platforms. Consequently, conducting such experiments is both feasible and promising on currently available Kitaev chain devices, utilizing existing control and measurement technologies. This would provide a crucial step toward the realization of the first Majorana qubit in solid-state systems. In fact, the observation of stable Rabi oscillations is synonymous with having a qubit, and our work establishes that such a qubit experiment should be successful in the existing Majorana platforms.

Acknowledgements.—We are particularly grateful to Xin Zhang, Francesco Zatelli, F. Setiawan, Michael Wimmer, and Jay D. Sau for useful discussions. H.P. is supported by US-ONR grant No. N00014-23-1-2357. C-X.L. is supported by a subsidy for top consortia for knowledge and innovation (TKI toeslag). S.D.S. is supported by the Laboratory for Physical Sciences through the Condensed Matter Theory Center at the University of Maryland.

* chunxiaoliu62@gmail.com

- [1] N. Read and Dmitry Green, “Paired states of fermions in two dimensions with breaking of parity and time-reversal symmetries and the fractional quantum hall effect,” *Phys. Rev. B* **61**, 10267–10297 (2000).
- [2] A Yu Kitaev, “Unpaired Majorana fermions in quantum wires,” *Physics-Uspekhi* **44**, 131 (2001).
- [3] Chetan Nayak, Steven H. Simon, Ady Stern, Michael Freedman, and Sankar Das Sarma, “Non-Abelian anyons and topological quantum computation,” *Rev. Mod. Phys.* **80**, 1083–1159 (2008).
- [4] Jason Alicea, “New directions in the pursuit of Majorana fermions in solid state systems,” *Rep. Prog. Phys.* **75**, 076501 (2012).
- [5] Martin Leijnse and Karsten Flensberg, “Introduction to topological superconductivity and Majorana fermions,” *Semicond. Sci. Technol.* **27**, 124003 (2012).
- [6] C.W.J. Beenakker, “Search for Majorana fermions in superconductors,” *Annu. Rev. Condens. Matter Phys.* **4**, 113–136 (2013).
- [7] Tudor D Stanescu and Sumanta Tewari, “Majorana fermions in semiconductor nanowires: fundamentals, modeling, and experiment,” *J. Phys.: Condens. Matter* **25**, 233201 (2013).
- [8] Jian-Hua Jiang and Si Wu, “Non-Abelian topological superconductors from topological semimetals and related systems under the superconducting proximity effect,” *J. Phys.: Condens. Matter* **25**, 055701 (2013).
- [9] Sankar Das Sarma, Michael Freedman, and Chetan Nayak, “Majorana zero modes and topological quantum computation,” *Npj Quantum Information* **1**, 15001 EP – (2015).
- [10] Steven R. Elliott and Marcel Franz, “Colloquium: Majorana fermions in nuclear, particle, and solid-state physics,” *Rev. Mod. Phys.* **87**, 137–163 (2015).
- [11] Masatoshi Sato and Satoshi Fujimoto, “Majorana fermions and topology in superconductors,” *J. Phys. Soc. Jpn.* **85**, 072001 (2016).
- [12] Masatoshi Sato and Yoichi Ando, “Topological superconductors: a review,” *Rep. Prog. Phys.* **80**, 076501 (2017).
- [13] R. M. Lutchyn, E. P. A. M. Bakkers, L. P. Kouwenhoven, P. Krogstrup, C. M. Marcus, and Y. Oreg, “Majorana zero modes in superconductor–semiconductor heterostructures,” *Nat. Rev. Mater.* **3**, 52–68 (2018).
- [14] Hao Zhang, Dong E. Liu, Michael Wimmer, and Leo P. Kouwenhoven, “Next steps of quantum transport in Majorana nanowire devices,” *Nat. Commun.* **10**, 5128 (2019).
- [15] Karsten Flensberg, Felix von Oppen, and Ady Stern, “Engineered platforms for topological superconductivity and majorana zero modes,” *Nature Reviews Materials* **6**, 944–958 (2021).
- [16] Sankar Das Sarma, “In search of majorana,” *Nature Physics* **19**, 165–170 (2023).
- [17] Jay D. Sau and S. Das Sarma, “Realizing a robust practical Majorana chain in a quantum-dot-superconductor linear array,” *Nat. Commun.* **3**, 964 (2012).
- [18] Haining Pan and S. Das Sarma, “Physical mechanisms for zero-bias conductance peaks in majorana nanowires,” *Phys. Rev. Res.* **2**, 013377 (2020).
- [19] Seongjin Ahn, Haining Pan, Benjamin Woods, Tudor D. Stanescu, and Sankar Das Sarma, “Estimating disorder and its adverse effects in semiconductor majorana nanowires,” *Phys. Rev. Mater.* **5**, 124602 (2021).
- [20] Sankar Das Sarma, Jay D. Sau, and Tudor D. Stanescu, “Spectral properties, topological patches, and effective phase diagrams of finite disordered majorana nanowires,” *Phys. Rev. B* **108**, 085416 (2023).
- [21] Sankar Das Sarma and Haining Pan, “Density of states, transport, and topology in disordered majorana nanowires,” *Phys. Rev. B* **108**, 085415 (2023).
- [22] Jacob R. Taylor, Jay D. Sau, and Sankar Das Sarma, “Machine learning the disorder landscape of majorana nanowires,” *Phys. Rev. Lett.* **132**, 206602 (2024).
- [23] Chun-Xiao Liu, Guanzhong Wang, Tom Dvir, and Michael Wimmer, “Tunable superconducting coupling of quantum dots via andreev bound states in semiconductor-superconductor nanowires,” *Phys. Rev. Lett.* **129**, 267701 (2022).
- [24] Alberto Bordin, Guanzhong Wang, Chun-Xiao Liu, Sebastiaan L. D. ten Haaf, Nick van Loo, Grzegorz P. Mazur, Di Xu, David van Driel, Francesco Zatelli, Sasa Gazibegovic, Ghada Badawy, Erik P. A. M. Bakkers, Michael Wimmer, Leo P. Kouwenhoven, and Tom Dvir, “Tunable crossed andreev reflection and elastic cotunneling in hybrid nanowires,” *Phys. Rev. X* **13**, 031031 (2023).

- [25] Guanzhong Wang, Tom Dvir, Grzegorz P. Mazur, Chun-Xiao Liu, Nick van Loo, Sebastiaan L. D. ten Haaf, Alberto Bordin, Sasa Gazibegovic, Ghada Badawy, Erik P. A. M. Bakkers, Michael Wimmer, and Leo P. Kouwenhoven, “Singlet and triplet cooper pair splitting in hybrid superconducting nanowires,” *Nature* **612**, 448–453 (2022).
- [26] Qingzhen Wang, Sebastiaan L. D. ten Haaf, Ivan Kulesh, Di Xiao, Candice Thomas, Michael J. Manfra, and Srijit Goswami, “Triplet correlations in cooper pair splitters realized in a two-dimensional electron gas,” *Nat. Commun.* **14**, 4876 (2023).
- [27] Alberto Bordin, Xiang Li, David van Driel, Jan Cornelis Wolff, Qingzhen Wang, Sebastiaan L. D. ten Haaf, Guanzhong Wang, Nick van Loo, Leo P. Kouwenhoven, and Tom Dvir, “Crossed andreev reflection and elastic cotunneling in three quantum dots coupled by superconductors,” *Phys. Rev. Lett.* **132**, 056602 (2024).
- [28] Martin Leijnse and Karsten Flensberg, “Parity qubits and poor man’s Majorana bound states in double quantum dots,” *Phys. Rev. B* **86**, 134528 (2012).
- [29] Tom Dvir, Guanzhong Wang, Nick van Loo, Chun-Xiao Liu, Grzegorz P. Mazur, Alberto Bordin, Sebastiaan L. D. ten Haaf, Ji-Yin Wang, David van Driel, Francesco Zatelli, Xiang Li, Filip K. Malinowski, Sasa Gazibegovic, Ghada Badawy, Erik P. A. M. Bakkers, Michael Wimmer, and Leo P. Kouwenhoven, “Realization of a minimal kitaev chain in coupled quantum dots,” *Nature* **614**, 445–450 (2023).
- [30] Francesco Zatelli, David van Driel, Di Xu, Guanzhong Wang, Chun-Xiao Liu, Alberto Bordin, Bart Roovers, Grzegorz P. Mazur, Nick van Loo, Jan Cornelis Wolff, *et al.*, “Robust poor man’s majorana zero modes using yu-shiba-rusinov states,” *arXiv:2311.03193* (2023).
- [31] Alberto Bordin, Chun-Xiao Liu, Tom Dvir, Francesco Zatelli, Sebastiaan LD ten Haaf, David van Driel, Guanzhong Wang, Nick van Loo, Thomas van Caekenberghe, Jan Cornelis Wolff, *et al.*, “Signatures of majorana protection in a three-site kitaev chain,” *arXiv:2402.19382* (2024).
- [32] Sebastiaan L. D. ten Haaf, Qingzhen Wang, A. Mert Bozkurt, Chun-Xiao Liu, Ivan Kulesh, Philip Kim, Di Xiao, Candice Thomas, Michael J. Manfra, Tom Dvir, Michael Wimmer, and Srijit Goswami, “A two-site kitaev chain in a two-dimensional electron gas,” *Nature* **630**, 329–334 (2024).
- [33] Jay D. Sau and Sankar Das Sarma, “Capacitance-based fermion parity read-out and predicted rabi oscillations in a majorana nanowire,” *arXiv:2406.18080* (2024).
- [34] Chun-Xiao Liu, Haining Pan, F. Setiawan, Michael Wimmer, and Jay D. Sau, “Fusion protocol for majorana modes in coupled quantum dots,” *Phys. Rev. B* **108**, 085437 (2023).
- [35] Péter Boross and András Pályi, “Braiding-based quantum control of a majorana qubit built from quantum dots,” *Phys. Rev. B* **109**, 125410 (2024).
- [36] Athanasios Tsintzis, Rubén Seoane Souto, Karsten Flensberg, Jeroen Danon, and Martin Leijnse, “Majorana qubits and non-abelian physics in quantum dot-based minimal kitaev chains,” *PRX Quantum* **5**, 010323 (2024).
- [37] V. Mourik, K. Zuo, S. M. Frolov, S.R. Plissard, E. P. A. M. Bakkers, and L. P. Kouwenhoven, “Signatures of Majorana fermions in hybrid semiconductor-semiconductor nanowire devices,” *Science* **336**, 1003–1007 (2012).
- [38] Fabrizio Nichele, Asbjørn C. C. Drachmann, Alexander M. Whiticar, Eoin C. T. O’Farrell, Henri J. Suominen, Antonio Fornieri, Tian Wang, Geoffrey C. Gardner, Candice Thomas, Anthony T. Hatke, Peter Krogstrup, Michael J. Manfra, Karsten Flensberg, and Charles M. Marcus, “Scaling of Majorana zero-bias conductance peaks,” *Phys. Rev. Lett.* **119**, 136803 (2017).
- [39] Hao Zhang, Michiel WA de Moor, Jouri DS Bommer, Di Xu, Guanzhong Wang, Nick van Loo, Chun-Xiao Liu, Sasa Gazibegovic, John A Logan, Diana Car, *et al.*, “Large zero-bias peaks in InSb-Al hybrid semiconductor-superconductor nanowire devices,” *arXiv:2101.11456* (2021).
- [40] Morteza Aghaee, Arun Akkala, Zulfi Alam, Rizwan Ali, Alejandro Alcaraz Ramirez, Mariusz Andrzejczuk, Andrey E. Antipov, Pavel Aseev, Mikhail Astafev, Bela Bauer, Jonathan Becker, Srinu Boddapati, Frenk Boekhout, Jouri Bommer, Tom Bosma, Leo Bourdet, Samuel Boutin, Philippe Caroff, Lucas Casparis, Maja Cassidy, Sohail Chatoor, Anna Wulf Christensen, Noah Clay, William S. Cole, Fabiano Corsetti, Ajuan Cui, Paschalis Dalampiras, Anand Dokania, Gijs de Lange, Michiel de Moor, Juan Carlos Estrada Saldaña, Saeed Fallahi, Zahra Heidarnia Fathabad, John Gamble, Geoff Gardner, Deshan Govender, Flavio Griggio, Ruben Grigoryan, Sergei Gronin, Jan Gukelberger, Esben Bork Hansen, Sebastian Heedt, Jesús Herranz Zamorano, Samantha Ho, Ulrik Laurens Holgaard, Henrik Ingerslev, Linda Johansson, Jeffrey Jones, Ray Kallaher, Farhad Karimi, Torsten Karzig, Evelyn King, Maren Elisabeth Kloster, Christina Knapp, Dariusz Kocou, Jonne Koski, Pasi Kostamo, Peter Krogstrup, Mahesh Kumar, Tom Laeven, Thorvald Larsen, Kongyi Li, Tyler Lindemann, Julie Love, Roman Lutchny, Morten Hannibal Madsen, Michael Manfra, Signe Markussen, Esteban Martinez, Robert McNeil, Elvedin Memisevic, Trevor Morgan, Andrew Mullally, Chetan Nayak, Jens Nielsen, William Hvidtfelt Padkær Nielsen, Bas Nijholt, Anne Nurmohamed, Eoin O’Farrell, Keita Otani, Sebastian Pauka, Karl Petersson, Luca Petit, Dmitry I. Pikulin, Frank Preiss, Marina Quintero-Perez, Mohana Rajpalke, Katrine Rasmussen, Davydas Razmadze, Outi Reentila, David Reilly, Richard Rouse, Ivan Sadovskyy, Lauri Sainiemi, Sydney Schreppler, Vadim Sidorkin, Amrita Singh, Shilpi Singh, Sarat Sinha, Patrick Sohr, Toma š Stankevič, Lieuwe Stek, Henri Suominen, Judith Suter, Vicky Svidenko, Sam Teicher, Mine Temuerhan, Nivetha Thiyagarajah, Raj Tholapi, Mason Thomas, Emily Toomey, Shivendra Upadhyay, Ivan Urban, Saulius Vaitiekėnas, Kevin Van Hoogdalem, David Van Wierkom, Dmitrii V. Viazmitinov, Dominik Vogel, Steven Waddy, John Watson, Joseph Weston, Georg W. Winkler, Chung Kai Yang, Sean Yau, Daniel Yi, Emrah Yuçelen, Alex Webster, Roland Zeisel, and Ruichen Zhao (Microsoft Quantum), “Inas-al hybrid devices passing the topological gap protocol,” *Phys. Rev. B* **107**, 245423 (2023).
- [41] Jay D. Sau, Roman M. Lutchny, Sumanta Tewari, and S. Das Sarma, “Generic new platform for topological quantum computation using semiconductor heterostructures,” *Phys. Rev. Lett.* **104**, 040502 (2010).
- [42] Roman M. Lutchny, Jay D. Sau, and S. Das Sarma,

- “Majorana fermions and a topological phase transition in semiconductor-superconductor heterostructures,” *Phys. Rev. Lett.* **105**, 077001 (2010).
- [43] Yuval Oreg, Gil Refael, and Felix von Oppen, “Helical liquids and Majorana bound states in quantum wires,” *Phys. Rev. Lett.* **105**, 177002 (2010).
- [44] Supplemental materials: I. Leakage probability in a Rabi experiment II. Dephasing time T_2 estimation III. Model Hamiltonian and parameters in the numerical simulations IV. Quantum capacitance measurement of a Majorana qubit.
- [45] Xuedong Hu and S. Das Sarma, “Charge-fluctuation-induced dephasing of exchange-coupled spin qubits,” *Phys. Rev. Lett.* **96**, 100501 (2006).
- [46] K. D. Petersson, J. R. Petta, H. Lu, and A. C. Gosard, “Quantum coherence in a one-electron semiconductor charge qubit,” *Phys. Rev. Lett.* **105**, 246804 (2010).
- [47] O. E. Dial, M. D. Shulman, S. P. Harvey, H. Bluhm, V. Umansky, and A. Yacoby, “Charge noise spectroscopy using coherent exchange oscillations in a singlet-triplet qubit,” *Phys. Rev. Lett.* **110**, 146804 (2013).
- [48] P. Scarlino, J. H. Ungerer, D. J. van Woerkom, M. Mancini, P. Stano, C. Müller, A. J. Landig, J. V. Koski, C. Reichl, W. Wegscheider, T. Ihn, K. Ensslin, and A. Wallraff, “In situ tuning of the electric-dipole strength of a double-dot charge qubit: Charge-noise protection and ultrastrong coupling,” *Phys. Rev. X* **12**, 031004 (2022).
- [49] Elliot J. Connors, J. Nelson, Lisa F. Edge, and John M. Nichol, “Charge-noise spectroscopy of si/sige quantum dots via dynamically-decoupled exchange oscillations,” *Nature Communications* **13**, 940 (2022).
- [50] Robert E. Throckmorton and S. Das Sarma, “Crosstalk and charge-noise-induced multiqubit decoherence in exchange-coupled quantum dot spin qubit arrays,” *Phys. Rev. B* **105**, 245413 (2022).
- [51] Guido Burkard, Thaddeus D. Ladd, Andrew Pan, John M. Nichol, and Jason R. Petta, “Semiconductor spin qubits,” *Rev. Mod. Phys.* **95**, 025003 (2023).
- [52] E. Paladino, Y. M. Galperin, G. Falci, and B. L. Altshuler, “ $1/f$ noise: Implications for solid-state quantum information,” *Rev. Mod. Phys.* **86**, 361–418 (2014).
- [53] G. Ithier, E. Collin, P. Joyez, P. J. Meeson, D. Vion, D. Esteve, F. Chiarello, A. Shnirman, Y. Makhlin, J. Schrieffer, and G. Schön, “Decoherence in a superconducting quantum bit circuit,” *Phys. Rev. B* **72**, 134519 (2005).
- [54] Péter Boross and András Pályi, “Dephasing of majorana qubits due to quasistatic disorder,” *Phys. Rev. B* **105**, 035413 (2022).
- [55] T. Hayashi, T. Fujisawa, H. D. Cheong, Y. H. Jeong, and Y. Hirayama, “Coherent manipulation of electronic states in a double quantum dot,” *Phys. Rev. Lett.* **91**, 226804 (2003).
- [56] Chun-Xiao Liu, A. Mert Bozkurt, Francesco Zatelli, Sebastiaan L. D. ten Haaf, Tom Dvir, and Michael Wimmer, “Enhancing the excitation gap of a quantum-dot-based kitaev chain,” *Communications Physics* **7**, 235 (2024).
- [57] Yu Luh, “Bound state in superconductors with paramagnetic impurities,” *Acta Physica Sinica* **21**, 75 (1965).
- [58] Hiroyuki Shiba, “Classical spins in superconductors,” *Progress of Theoretical Physics* **40**, 435–451 (1968).
- [59] AI Rusinov, “Theory of gapless superconductivity in alloys containing paramagnetic impurities,” *Sov. Phys. JETP* **29**, 1101–1106 (1969).
- [60] Morteza Aghaee, Alejandro Alcaraz Ramirez, Zulf Alam, Rizwan Ali, Mariusz Andrzejczuk, Andrey Antipov, Mikhail Astafev, Amin Barzegar, Bela Bauer, Jonathan Becker, *et al.*, “Interferometric single-shot parity measurement in an inas-al hybrid device,” [arXiv:2401.09549](https://arxiv.org/abs/2401.09549) (2024).
- [61] Chun-Xiao Liu, Sebastian Miles, Alberto Bordin, Sebastiaan LD ten Haaf, A Mert Bozkurt, and Michael Wimmer, “Protocol for scaling up a sign-ordered kitaev chain without magnetic flux control,” [arXiv:2407.04630](https://arxiv.org/abs/2407.04630) (2024).

Supplemental Materials for “Rabi oscillation and coherence time of Majorana qubit in quantum dot-superconductor array”

Appendix I: Leakage probability in a Rabi experiment

The system of the double two-site Kitaev chain is described by the following Hamiltonian:

$$\mathcal{H}_{\text{tot}} = \mathcal{H}_L + \mathcal{H}_R + \mathcal{H}_T + \mathcal{H}_\mu \quad (\text{S-1})$$

where intra-chain coupling in the left chain (Site index 1 and 2) and right chain (Site index 3 and 4) are

$$\begin{aligned} \mathcal{H}_L &= t \sum \left(c_{L2}^\dagger c_{L1} + c_{L1}^\dagger c_{L2} \right) + \Delta \left(c_{L2} c_{L1} + c_{L1}^\dagger c_{L2}^\dagger \right) \\ \mathcal{H}_R &= t \sum \left(c_{R2}^\dagger c_{R1} + c_{R1}^\dagger c_{R2} \right) + \Delta \left(c_{R2} c_{R1} + c_{R1}^\dagger c_{R2}^\dagger \right), \end{aligned} \quad (\text{S-2})$$

the inter-chain hopping is

$$\mathcal{H}_T = \Gamma \left(c_{R1}^\dagger c_{L2} + c_{L2}^\dagger c_{R1} \right), \quad (\text{S-3})$$

and the onsite chemical potential is

$$\mathcal{H}_\mu = \sum_{a \in \{L,R\}} \sum_{i=1}^2 \mu_{a,i} c_{a,i}^\dagger c_{a,i}. \quad (\text{S-4})$$

Up to a particle-hole transformation, we can choose $t > 0$, $\Delta > 0$, and $\Gamma > 0$.

Here, without the tunneling term $\Gamma = 0$, the two chains are decoupled, where the sweet spot is achieved when $t = \Delta$, and $\mu_{a,i} = 0$, leading to the ground state manifold spanned by

$$|e\rangle_L = \frac{1}{\sqrt{2}} \left(1 - c_{L1}^\dagger c_{L2}^\dagger \right) |0\rangle, |o\rangle_L = \frac{1}{\sqrt{2}} \left(c_{L1}^\dagger - c_{L2}^\dagger \right) |0\rangle, \quad (\text{S-5})$$

$$|e\rangle_R = \frac{1}{\sqrt{2}} \left(1 - c_{R1}^\dagger c_{R2}^\dagger \right) |0\rangle, |o\rangle_R = \frac{1}{\sqrt{2}} \left(c_{R1}^\dagger - c_{R2}^\dagger \right) |0\rangle, \quad (\text{S-6})$$

for the left and right systems, respectively.

With the tunneling term, the ground state of the two chains can be spanned by the two other single-chain excited states denoted as

$$|e'\rangle_L = \frac{1}{\sqrt{2}} \left(1 + c_{L1}^\dagger c_{L2}^\dagger \right) |0\rangle, |o'\rangle_L = \frac{1}{\sqrt{2}} \left(c_{L1}^\dagger + c_{L2}^\dagger \right) |0\rangle, \quad (\text{S-7})$$

$$|e'\rangle_R = \frac{1}{\sqrt{2}} \left(1 + c_{R1}^\dagger c_{R2}^\dagger \right) |0\rangle, |o'\rangle_R = \frac{1}{\sqrt{2}} \left(c_{R1}^\dagger + c_{R2}^\dagger \right) |0\rangle. \quad (\text{S-8})$$

Therefore, $|e\rangle_L, |e'\rangle_L, |o\rangle_L$, and $|o'\rangle_L$ ($|e\rangle_R, |e'\rangle_R, |o\rangle_R$, and $|o'\rangle_R$) form the complete basis for the left (right) chain.

Without the loss of generality, we choose to work in the even-total-parity, leading to a complete basis of $|ee\rangle \equiv |e\rangle_L |e\rangle_R, |oo\rangle, |e'e'\rangle, |o'o'\rangle, |ee'\rangle, |oo'\rangle, |e'e\rangle$, and $|o'o\rangle$. With this set of bases, the matrix representation of the sum of Hamiltonian Eq. (S-2) and Eq. (S-3) is

$$H_L + H_R + H_T = \begin{pmatrix} h_+ & 0 \\ 0 & h_- \end{pmatrix}, \quad (\text{S-9})$$

where h_+ and h_- are

$$h_+ = \begin{pmatrix} -2\Delta & -\Gamma/2 & 0 & -\Gamma/2 \\ -\Gamma/2 & -2t & \Gamma/2 & 0 \\ 0 & \Gamma/2 & 2\Delta & \Gamma/2 \\ -\Gamma/2 & 0 & \Gamma/2 & 2t \end{pmatrix}, \quad (\text{S-10})$$

$$h_- = \begin{pmatrix} 0 & \Gamma/2 & 0 & \Gamma/2 \\ \Gamma/2 & 0 & -\Gamma/2 & 0 \\ 0 & -\Gamma/2 & 0 & -\Gamma/2 \\ \Gamma/2 & 0 & -\Gamma/2 & 0 \end{pmatrix}. \quad (\text{S-11})$$

Similarly, the matrix representation of the onsite chemical potential Eq. (S-4) is

$$H_\mu = \frac{\mu_{LR}}{2} \mathbf{1} + \frac{1}{2} \begin{pmatrix} 0 & h_\mu \\ h_\mu^\dagger & 0 \end{pmatrix}, \quad (\text{S-12})$$

where

$$h_\mu = \begin{pmatrix} -\mu_R & 0 & -\mu_L & 0 \\ 0 & \delta\mu_R & 0 & \delta\mu_L \\ -\mu_L & 0 & -\mu_R & 0 \\ 0 & \delta\mu_L & 0 & \delta\mu_R \end{pmatrix}, \quad (\text{S-13})$$

with the shorthand notions of $\mu_{LR} \equiv \sum_{a \in \{L,R\}} \mu_a$, $\mu_a \equiv \mu_{a1} + \mu_{a2}$, and $\delta\mu_a \equiv \mu_{a1} - \mu_{a2}$.

1. Leakage due to Δ , t , and Γ

In Eq. (2) in the main text, we considered the disorder effect in ϵ and Γ before σ_z and σ_x . Here, we will consider their leakage effect separately to understand the leakage that is effectively on ϵ and Γ .

We first consider the effect of the disorder only in Δ , t , and Γ , i.e., $\mu_{a,i} = 0$, because Eq. (S-9) is block diagonal, and given the initial state being $|ee\rangle$, we only need to consider the subspace of h_+ , where the Rabi oscillation is between $|ee\rangle$ and $|oo\rangle$, and the leakage states are $|e'e'\rangle$ and $|o'o'\rangle$.

We use the time-dependent perturbation theory, where Eq. (S-9) is decomposed into the noninteracting part H_0

$$H_0 = \begin{pmatrix} -2\Delta & -\Gamma/2 & 0 & 0 \\ -\Gamma/2 & -2t & 0 & 0 \\ 0 & 0 & 2\Delta & \Gamma/2 \\ 0 & 0 & \Gamma/2 & 2t \end{pmatrix}, \quad (\text{S-14})$$

and the perturbation H_1 as

$$H_1 = \begin{pmatrix} 0 & 0 & 0 & -\Gamma/2 \\ 0 & 0 & \Gamma/2 & 0 \\ 0 & \Gamma/2 & 0 & 0 \\ -\Gamma/2 & 0 & 0 & 0 \end{pmatrix}. \quad (\text{S-15})$$

Conceptually, the first term H_0 in Eq. (S-14) accounts for the Rabi oscillation between $|ee\rangle$ and $|oo\rangle$ (given the initial state being $|ee\rangle$), and the second term H_1 in Eq. (S-15) leads to $|e'e'\rangle$ and $|o'o'\rangle$.

The time evolution operator (in the Schrödinger picture) is expanded in the Dyson series (truncated at the first order) as

$$U(\tau) = e^{-iH_0\tau} \left(1 - i \int_0^\tau d\tau_1 H_{1,I}(\tau_1) \right) e^{iH_0\tau}, \quad (\text{S-16})$$

where $H_{1,I}(\tau_1)$ is H_1 in the interacting picture

$$H_{1,I}(\tau_1) = e^{iH_0\tau_1} H_1 e^{-iH_0\tau_1} = \sum_{i,j} \langle i | H_1 | j \rangle e^{i(E_i - E_j)\tau_1}, \quad (\text{S-17})$$

and $|i\rangle$ is the eigenvector of H_0 with the eigenvalues of E_i .

The spectrum of H_0 in Eq. (S-14) is

$$\begin{aligned} -E_+ &: \left(\cos\left(\frac{\theta}{2}\right) \sin\left(\frac{\theta}{2}\right) 0 0 \right)^\top \\ -E_- &: \left(-\sin\left(\frac{\theta}{2}\right) \cos\left(\frac{\theta}{2}\right) 0 0 \right)^\top \\ E_- &: \left(0 0 -\sin\left(\frac{\theta}{2}\right) \cos\left(\frac{\theta}{2}\right) \right)^\top \\ E_+ &: \left(0 0 \cos\left(\frac{\theta}{2}\right) \sin\left(\frac{\theta}{2}\right) \right)^\top \end{aligned} \quad (\text{S-18})$$

where $E_\pm = \Delta + t \pm \sqrt{(\Delta - t)^2 + (\Gamma/2)^2}$, and $\tan \theta = \frac{\Gamma/2}{\Delta - t}$. We substitute the eigenvectors and eigenvalues of H_0 into Eq. (S-17), with the initial state

$$|\psi(\tau = 0)\rangle = |ee\rangle = (1 \ 0 \ 0 \ 0)^\top, \quad (\text{S-19})$$

we have the (unnormalized) final state in the Schrödinger picture as

$$|\psi(\tau)\rangle = U(\tau) |\psi(\tau = 0)\rangle = |\psi(\tau)\rangle = \begin{pmatrix} e^{i\omega\tau} [\cos(\Omega\tau) + i \sin(\Omega\tau) \cos \theta] \\ e^{i\omega\tau} i \sin(\Omega\tau) \sin \theta \\ \frac{\Gamma}{2\omega} \sin(\omega\tau) \sin(\Omega\tau) \sin \theta \\ \frac{\Gamma}{2\omega} [-\sin(\Omega\tau) \cos \theta + i \cos(\Omega\tau)] \sin(\omega\tau) \end{pmatrix}, \quad (\text{S-20})$$

where $\Omega = \sqrt{(\Delta - t)^2 + (\Gamma/2)^2}$ and $\omega = \Delta + t$.

Therefore, the Rabi oscillation between $|ee\rangle$ and $|oo\rangle$ have the probability densities of

$$\begin{aligned} P_{ee}(\tau) &= |\langle ee|\psi(\tau)\rangle|^2 = \sin^2(\Omega\tau) \cos^2(\theta) + \cos^2(\Omega\tau) \\ P_{oo}(\tau) &= |\langle oo|\psi(\tau)\rangle|^2 = \sin^2(\theta) \sin^2(\Omega\tau), \end{aligned} \quad (\text{S-21})$$

and the leakage is

$$P_{\text{leak}}(\tau) = P_{e'e'}(\tau) + P_{o'o'}(\tau) = |\langle e'e'|\psi(\tau)\rangle|^2 + |\langle o'o'|\psi(\tau)\rangle|^2 = \frac{\Gamma^2 \sin^2(\omega\tau)}{4\omega^2}, \quad (\text{S-22})$$

indicating that the leakage frequency is $2\omega = 2(\Delta + t)$, which is independent of the Γ , and consistent with Fig. 2(b) in the main text.

Specifically, at the sweep spot $\Delta = t$, we have $\theta = \pi/2$ and the probability densities are

$$\begin{aligned} P_{ee}(\tau) &= \cos^2(\Omega\tau) \\ P_{oo}(\tau) &= \sin^2(\Omega\tau) \\ P_{\text{leak}}(\tau) &= \frac{\Gamma^2}{16\Delta^2} \sin^2(2\Delta\tau), \end{aligned} \quad (\text{S-23})$$

recovering the Rabi frequency $2\Omega = \Gamma$ in Frg. 2(a).

2. Leakage due to μ_{L1}

To consider the leakage effect in μ_{L1} (or, equivalently for μ_{R2} due to the inversion symmetry), we set all other parameters to the sweet spot, including $\Delta = t_0$ and $\mu_{L2} = \mu_{R1} = \mu_{R2} = 0$. Following the same time-dependent perturbation theory, the noninteracting part $H_0^{\mu_{L1}}$ is

$$H_0^{\mu_{L1}} = \frac{\mu_{L1}}{2} \mathbb{1} + \begin{pmatrix} H_0 & 0 \\ 0 & h_- \end{pmatrix} \quad (\text{S-24})$$

where H_0 and h_- are in Eq. (S-14) and in Eq. (S-11) (with $\Delta = t$), and the perturbation term $H_1^{\mu_{L1}}$ is

$$H_1^{\mu_{L1}} = \begin{pmatrix} H_1 & h_{\mu_{L1}} \\ h_{\mu_{L1}}^\dagger & 0 \end{pmatrix} \quad (\text{S-25})$$

where H_1 is in Eq. (S-15) and $H_{\mu_{L1}}$ is

$$h_{\mu_{L1}} = \frac{1}{2} \begin{pmatrix} 0 & 0 & -\mu_{L1} & 0 \\ 0 & 0 & 0 & \mu_{L1} \\ -\mu_{L1} & 0 & 0 & 0 \\ 0 & \mu_{L1} & 0 & 0 \end{pmatrix}. \quad (\text{S-26})$$

from Eq. (S-13).

Here, the noninteracting term $H_0^{\mu_{L1}}$ has the eigenvalues and eigenvectors as

$$\begin{aligned} -2\Delta - \frac{\Gamma}{2} + \frac{\mu_1}{2} &: \frac{1}{\sqrt{2}} (1 \ 1 \ 0 \ 0 \ 0 \ 0 \ 0 \ 0)^\top \\ -2\Delta + \frac{\Gamma}{2} + \frac{\mu_1}{2} &: \frac{1}{\sqrt{2}} (-1 \ 1 \ 0 \ 0 \ 0 \ 0 \ 0 \ 0)^\top \\ 2\Delta - \frac{\Gamma}{2} + \frac{\mu_1}{2} &: \frac{1}{\sqrt{2}} (0 \ 0 \ -1 \ 1 \ 0 \ 0 \ 0 \ 0)^\top \\ 2\Delta + \frac{\Gamma}{2} + \frac{\mu_1}{2} &: \frac{1}{\sqrt{2}} (0 \ 0 \ 1 \ 1 \ 0 \ 0 \ 0 \ 0)^\top \\ \frac{\mu_1}{2} &: \frac{1}{\sqrt{2}} (0 \ 0 \ 0 \ 0 \ 1 \ 0 \ 1 \ 0)^\top \\ \frac{\mu_1}{2} &: \frac{1}{\sqrt{2}} (0 \ 0 \ 0 \ 0 \ 0 \ -1 \ 0 \ 1)^\top \\ -\Gamma + \frac{\mu_1}{2} &: \frac{1}{2} (0 \ 0 \ 0 \ 0 \ 1 \ 1 \ -1 \ 1)^\top \\ \Gamma + \frac{\mu_1}{2} &: \frac{1}{2} (0 \ 0 \ 0 \ 0 \ -1 \ 1 \ 1 \ 1)^\top \end{aligned} \quad (\text{S-27})$$

With the initial state being $|ee\rangle = (1 \ 0 \ 0 \ 0 \ 0 \ 0 \ 0 \ 0)^\top$, the (unnormalized) final state in the Schrödinger picture is

$$\psi^{\mu_{L1}}(\tau) = \begin{pmatrix} e^{i\tau(2\Delta - \frac{\mu_1}{2})} \cos\left(\frac{\tau\Gamma}{2}\right) \\ ie^{i\tau(2\Delta - \frac{\mu_1}{2})} \sin\left(\frac{\tau\Gamma}{2}\right) \\ \frac{\Gamma}{4\Delta} e^{-\frac{i\tau\mu_1}{2}} \sin(2\tau\Delta) \sin\left(\frac{\tau\Gamma}{2}\right) \\ \frac{i\Gamma}{4\Delta} e^{-\frac{i\tau\mu_1}{2}} \sin(2\tau\Delta) \cos\left(\frac{\tau\Gamma}{2}\right) \\ \frac{1}{2}\mu_1 e^{i\tau(\Delta - \frac{\mu_1}{2})} \sin\left(\frac{\tau\Gamma}{2}\right) \left(\frac{1}{E_-} e^{\frac{i\tau\Gamma}{4}} \sin\left(\frac{E_- \tau}{2}\right) - \frac{1}{E_+} e^{-\frac{i\tau\Gamma}{4}} \sin\left(\frac{E_+ \tau}{2}\right) \right) \\ \frac{1}{2}\mu_1 e^{i\tau(\Delta - \frac{\mu_1}{2})} \cos\left(\frac{\tau\Gamma}{2}\right) \left(-\frac{1}{E_-} ie^{\frac{i\tau\Gamma}{4}} \sin\left(\frac{E_- \tau}{2}\right) + \frac{1}{E_+} ie^{-\frac{i\tau\Gamma}{4}} \sin\left(\frac{E_+ \tau}{2}\right) \right) \\ \frac{1}{2}\mu_1 e^{i\tau(\Delta - \frac{\mu_1}{2})} \cos\left(\frac{\tau\Gamma}{2}\right) \left(\frac{1}{E_-} ie^{\frac{i\tau\Gamma}{4}} \sin\left(\frac{E_- \tau}{2}\right) + \frac{1}{E_+} ie^{-\frac{i\tau\Gamma}{4}} \sin\left(\frac{E_+ \tau}{2}\right) \right) \\ \frac{1}{2}\mu_1 e^{i\tau(\Delta - \frac{\mu_1}{2})} \sin\left(\frac{\tau\Gamma}{2}\right) \left(\frac{1}{E_-} e^{\frac{i\tau\Gamma}{4}} \sin\left(\frac{E_- \tau}{2}\right) + \frac{1}{E_+} e^{-\frac{i\tau\Gamma}{4}} \sin\left(\frac{E_+ \tau}{2}\right) \right) \end{pmatrix}, \quad (\text{S-28})$$

where $E_{\pm} = 2\Delta \pm \Gamma/2$.

Therefore, the leakage to the $|e'e'\rangle$ and $|o'o'\rangle$ is the same

$$P_{e'e'}(\tau) + P_{o'o'}(\tau) = |\langle e'e' | \psi^{\mu_{L1}}(\tau) \rangle|^2 + |\langle o'o' | \psi^{\mu_{L1}}(\tau) \rangle|^2 = \frac{\Gamma^2 \sin^2(2\tau\Delta)}{16\Delta^2}, \quad (\text{S-29})$$

and the leakage to $|ee'\rangle$, $|oo'\rangle$, $|e'e\rangle$, and $|o'o\rangle$ is

$$\begin{aligned} P_{ee'}(\tau) + P_{oo'}(\tau) + P_{e'e}(\tau) + P_{o'o}(\tau) &= |\langle ee' | \psi^{\mu_{L1}}(\tau) \rangle|^2 + |\langle oo' | \psi^{\mu_{L1}}(\tau) \rangle|^2 + |\langle e'e | \psi^{\mu_{L1}}(\tau) \rangle|^2 + |\langle o'o | \psi^{\mu_{L1}}(\tau) \rangle|^2 \\ &= \frac{\mu_{L1}^2}{2} \left(\frac{\sin^2\left(\frac{E_- \tau}{2}\right)}{E_-^2} + \frac{\sin^2\left(\frac{E_+ \tau}{2}\right)}{E_+^2} \right), \end{aligned} \quad (\text{S-30})$$

This introduces a superposition of two frequencies E_- and E_+ in the leakage frequency, where the envelope frequency is $E_- + E_+ = 4\Delta$ and the carrier frequency is $E_+ - E_- = \Gamma$.

3. Leakage due to μ_{L2}

The leakage effect in the other onsite chemical potential is μ_{L2} (or μ_{R1}). Namely, we set $\mu_{L1} = \mu_{R1} = \mu_{R2} = 0$, and $t = \Delta$. This leads to the same noninteracting part $H_0^{\mu_{L2}} = H_0^{\mu_{L1}}$ as in Eq. (S-24), while the perturbation term $H_1^{\mu_{L2}}$ is

$$H_1^{\mu_{L2}} = \begin{pmatrix} H_1 & h_{\mu_{L2}} \\ h_{\mu_{L2}}^\dagger & 0 \end{pmatrix} \quad (\text{S-31})$$

where H_1 is in Eq. (S-15) and $h_{\mu_{L2}}$ is

$$h_{\mu_{L2}} = \frac{1}{2} \begin{pmatrix} 0 & 0 & -\mu_{L2} & 0 \\ 0 & 0 & 0 & -\mu_{L2} \\ -\mu_{L2} & 0 & 0 & 0 \\ 0 & -\mu_{L2} & 0 & 0 \end{pmatrix} \quad (\text{S-32})$$

Here, the noninteracting term $H_0^{\mu_{L2}}$ has the same eigenvalues (with μ_{L1} replaced with μ_{L2}) and eigenvectors as in Eq. (S-27), and therefore, the final state in the Schrödinger picture starting from $|ee\rangle$ is

$$\psi^{\mu_{L2}}(\tau) = \begin{pmatrix} e^{i\tau(2\Delta - \frac{\mu_2}{2})} \cos\left(\frac{\tau\Gamma}{2}\right) \\ ie^{i\tau(2\Delta - \frac{\mu_2}{2})} \sin\left(\frac{\tau\Gamma}{2}\right) \\ \frac{\Gamma}{4\Delta} e^{-\frac{i\tau\mu_2}{2}} \sin(2\tau\Delta) \sin\left(\frac{\tau\Gamma}{2}\right) \\ \frac{i\Gamma}{4\Delta} e^{-\frac{i\tau\mu_2}{2}} \sin(2\tau\Delta) \cos\left(\frac{\tau\Gamma}{2}\right) \\ \left[\begin{array}{l} \frac{\mu_2}{4} e^{i\tau(\Delta - \frac{\mu_2}{2})} \left[\left(\frac{i \sin\left(\frac{E_- \tau}{2}\right)}{E_-} - \frac{i \sin\left(\frac{E'_+ \tau}{2}\right)}{E'_+} \right) e^{-\frac{i\tau\Gamma}{4}} + \left(-\frac{i \sin\left(\frac{E'_- \tau}{2}\right)}{E'_-} + \frac{i \sin\left(\frac{E_+ \tau}{2}\right)}{E_+} \right) e^{\frac{i\tau\Gamma}{4}} \right] \\ \frac{\mu_2}{4} e^{i\tau(\Delta - \frac{\mu_2}{2})} \left[\left(\frac{i \sin\left(\frac{E_- \tau}{2}\right)}{E_-} + \frac{i \sin\left(\frac{E'_+ \tau}{2}\right)}{E'_+} \right) e^{-\frac{i\tau\Gamma}{4}} + \left(-\frac{i \sin\left(\frac{E'_- \tau}{2}\right)}{E'_-} - \frac{i \sin\left(\frac{E_+ \tau}{2}\right)}{E_+} \right) e^{\frac{i\tau\Gamma}{4}} \right] \\ \frac{\mu_2}{4} e^{i\tau(\Delta - \frac{\mu_2}{2})} \left[\left(\frac{i \sin\left(\frac{E_- \tau}{2}\right)}{E_-} + \frac{i \sin\left(\frac{E'_+ \tau}{2}\right)}{E'_+} \right) e^{-\frac{i\tau\Gamma}{4}} + \left(\frac{i \sin\left(\frac{E'_- \tau}{2}\right)}{E'_-} + \frac{i \sin\left(\frac{E_+ \tau}{2}\right)}{E_+} \right) e^{\frac{i\tau\Gamma}{4}} \right] \\ \frac{\mu_2}{4} e^{i\tau(\Delta - \frac{\mu_2}{2})} \left[\left(-\frac{i \sin\left(\frac{E_- \tau}{2}\right)}{E_-} + \frac{i \sin\left(\frac{E'_+ \tau}{2}\right)}{E'_+} \right) e^{-\frac{i\tau\Gamma}{4}} + \left(-\frac{i \sin\left(\frac{E'_- \tau}{2}\right)}{E'_-} + \frac{i \sin\left(\frac{E_+ \tau}{2}\right)}{E_+} \right) e^{\frac{i\tau\Gamma}{4}} \right] \end{array} \right] \end{pmatrix}, \quad (\text{S-33})$$

where $E_{\pm} = 2\Delta \pm \Gamma/2$ and $E'_{\pm} = 2\Delta \pm 3\Gamma/2$.

Therefore, the leakage to the $|e'e'\rangle$ and $|o'o'\rangle$ is the same as Eq. (S-30), and the leakage to $|ee'\rangle$, $|oo'\rangle$, $|e'e\rangle$, and $|o'o\rangle$ is

$$\begin{aligned} P_{ee'}(\tau) + P_{oo'}(\tau) + P_{e'e}(\tau) + P_{o'o}(\tau) &= |\langle ee' | \psi^{\mu_{L2}}(\tau) \rangle|^2 + |\langle oo' | \psi^{\mu_{L2}}(\tau) \rangle|^2 + |\langle e'e | \psi^{\mu_{L2}}(\tau) \rangle|^2 + |\langle o'o | \psi^{\mu_{L2}}(\tau) \rangle|^2 \\ &= \frac{\mu_{L2}^2}{4} \left(\frac{\sin^2\left(\frac{E_- \tau}{2}\right)}{E_-^2} + \frac{\sin^2\left(\frac{E_+ \tau}{2}\right)}{E_+^2} + \frac{\sin^2\left(\frac{E'_- \tau}{2}\right)}{E'^-{}^2} + \frac{\sin^2\left(\frac{E'_+ \tau}{2}\right)}{E'^+{}^2} \right). \end{aligned} \quad (\text{S-34})$$

Appendix II: Dephasing time T_2 estimation

1. Dephasing due to disorder in Γ

In this section, we consider the dephasing effect which is used to estimate T_2 . To focus only on the low energy sector, we work in the minimal 2-level system where the Hilbert space only includes $|ee\rangle$ and $|oo\rangle$. The effect of Γ

acts like the magnetic field along the x direction, and therefore, the effective two-level Hamiltonian is

$$H_x = B_x \sigma_x, \quad (\text{S-1})$$

where B_x is quasi-static disorder following the Gaussian distribution with the variance of $\sigma_{B_x}^2$ and mean of \bar{B}_x , i.e., $B_x \sim \mathcal{N}(\bar{B}_x, \sigma_{B_x}^2)$, σ_x is the Pauli X matrix, and the initial state is $\psi_x(\tau = 0) = |ee\rangle$.

Under the evolution of H_x , the final state $\psi_x(\tau)$ is

$$\psi_x(\tau) = e^{-iH_x\tau} \psi_x(\tau = 0) = \begin{pmatrix} \cos(B_x\tau) \\ -i \sin(B_x\tau) \end{pmatrix}, \quad (\text{S-2})$$

Therefore, the probability of finding the state in $|oo\rangle$ is

$$P_{oo}(\tau) = |\langle oo | \psi_x(\tau) \rangle|^2 = \sin^2(B_x\tau). \quad (\text{S-3})$$

Thus, the disorder-averaged probability is

$$\langle P_{oo}(\tau) \rangle_{B_x} = \frac{1}{\sqrt{2\pi}\sigma_{B_x}} \int_{-\infty}^{\infty} dB_x e^{-\frac{(B_x - \bar{B}_x)^2}{2\sigma_{B_x}^2}} \sin^2(B_x\tau) = \frac{1}{2} \left[1 + e^{-2\tau^2\sigma_{B_x}^2} \cos(2\bar{B}_x\tau) \right]. \quad (\text{S-4})$$

Therefore, the decay of the envelope of $\langle P_{oo}(\tau) \rangle_{B_x}$ follows the Gaussian decay with a prefactor of $e^{-2\tau^2\sigma_{B_x}^2}$, namely, $\beta = 2$ in the ansatz in Eq. (5) in the main text. This provides a fundamental understanding of the ansatz in Eq. (5) in the main text.

2. Dephasing due to disorder in $\mu_{a,i}$, Δ , and t

Besides the dephasing effect due to the disorder in Γ , we also consider the dephasing effect due to the disorder in $\mu_{a,i}$, Δ , and t .

In practice, the disorder of these quantities acts like the magnetic field along the z direction, and therefore, the effective two-level Hamiltonian is

$$H_{xz} = B_x \sigma_x + B_z \sigma_z, \quad (\text{S-5})$$

where B_x here is constant, and B_z is quasi-static disorder following the Gaussian distribution with the variance of $\sigma_{B_z}^2$ and mean of 0, i.e., $B_z \sim \mathcal{N}(0, \sigma_{B_z}^2)$, σ_z is the Pauli Z matrix, and the initial state is again $\psi_{xz}(\tau = 0) = |ee\rangle$.

Under the evolution of H_{xz} , the final state $\psi_{xz}(\tau)$ is

$$\psi_{xz}(\tau) = e^{-iH_{xz}\tau} \psi_{xz}(\tau = 0) = \begin{pmatrix} \cos(\sqrt{B_x^2 + B_z^2}\tau) - i \sin(\sqrt{B_x^2 + B_z^2}\tau) \cos(\theta) \\ -i \sin(\sqrt{B_x^2 + B_z^2}\tau) \sin(\theta) \end{pmatrix}, \quad (\text{S-6})$$

where $\tan \theta = B_x/B_z$, and the probability of finding the state in $|oo\rangle$ is

$$P_{oo}(\tau) = |\langle oo | \psi_{xz}(\tau) \rangle|^2 = \sin^2(\sqrt{B_x^2 + B_z^2}\tau) \frac{B_x^2}{B_x^2 + B_z^2}. \quad (\text{S-7})$$

Therefore, the disorder-averaged probability is

$$\begin{aligned} \langle P_{oo}(\tau) \rangle_{B_z} &= \frac{1}{\sqrt{2\pi}\sigma_{B_z}} \int_{-\infty}^{\infty} dB_z e^{-\frac{B_z^2}{2\sigma_{B_z}^2}} \sin^2(\sqrt{B_x^2 + B_z^2}\tau) \frac{B_x^2}{B_x^2 + B_z^2} \\ &\approx \frac{1}{\sqrt{2\pi}\sigma_{B_z}} \int_{-\infty}^{\infty} dB_z e^{-\frac{B_z^2}{2\sigma_{B_z}^2}} \sin^2\left(\left(B_x^2 + \frac{B_z^2}{2B_x}\right)\tau\right) \\ &= \frac{1}{4} \left(2 - \frac{B_x e^{2iB_x\tau}}{\sqrt{B_x(B_x - 2i\sigma_{B_z}^2\tau)}} - \frac{B_x e^{-2iB_x\tau}}{\sqrt{B_x(B_x + 2i\sigma_{B_z}^2\tau)}} \right) \end{aligned} \quad (\text{S-8})$$

where the second line assumes the $B_z \ll B_x$ such that $\sqrt{B_x^2 + B_z^2} \approx B_x + \frac{B_z^2}{2B_x}$, and $\frac{B_x^2}{B_x^2 + B_z^2} \approx 1$. Therefore, it shows a power-law decay with $\langle P_{oo}(\tau) \rangle_{B_z} \sim \tau^{-\frac{1}{2}}$.

Appendix III: Model Hamiltonian and parameters in the numerical simulations

1. Model parameters for charge noises

In the numerical simulations of the Rabi and Ramsey oscillations shown in the main text, we include charge noises assuming quasi-static disorder. That is, the fluctuations of a model parameter λ follows an uncorrelated Gaussian distribution $\lambda \sim \mathcal{N}(\bar{\lambda}, \sigma_\lambda^2)$. In particular, in a charge qubit, the fluctuation amplitude of a dot level $\varepsilon_{L,R}$ is chosen to be $\sigma_\varepsilon = 3 \mu\text{eV}$ and for tunnel couplings we choose $\sigma_\Gamma/\Gamma = 0.01$ corresponding to the devices studied in Refs. [52, 55]. Other parameters for the charge qubit are summarized in Table II.

Supplementary Table II. Parameters for charge qubits in μeV .

Qubit	Protocol	$\bar{\Gamma}$	$\bar{\varepsilon}_L$	$\bar{\varepsilon}_R$	σ_ε	σ_Γ	Figure
Charge	Rabi	5	0	0	3	0.05	Fig. 3(a)
Charge	Ramsey x pulse	5	0	0	3	0.05	Fig. 3(d)
	Ramsey z pulse	5	20	-20	3	0.05	

The parameters of a Majorana qubit are chosen according to Refs. [29, 30, 32]. In a small-gap Majorana qubit, the fluctuation amplitudes of the dot orbitals are identical to those in double quantum dots, i.e. $\sigma_\mu = 3 \mu\text{eV}$. The intra-chain couplings are $t = \Delta = 12 \mu\text{eV}$ with a fluctuation amplitude $\sigma_t = 0.016 \mu\text{eV}$. The inter-chain couplings are chosen to be $\sigma_\Gamma/\Gamma = 0.01$, similar to charge qubits. In a large-gap Majorana qubit, since the dot charges are now significantly screened due to strong dot-superconductor hybridization [30, 56], the fluctuation amplitude reduces to only one-tenth of the normal dot, i.e. $\sigma_\mu = 0.3 \mu\text{eV}$. The intra-chain coupling strengths are now $t = \Delta = 38 \mu\text{eV}$ with fluctuations of $\sigma_t = 0.05 \mu\text{eV}$. The inter-chain coupling fluctuations are still chosen to be $\sigma_\Gamma/\Gamma = 0.01$. The other parameters for Majorana qubit parameters are summarized in Table III.

Supplementary Table III. Parameters for Majorana qubits in μeV .

Qubit	Protocol	\bar{t}_a	Δ_a	$\bar{\Gamma}$	$\bar{\mu}_{ai}$	σ_t	σ_μ	σ_Γ	Figure
Small-gap Majorana	Rabi	12	12	5	0	0.016	3	0.05	Fig. 3(b)
Large-gap Majorana	Rabi	38	38	5	0	0.05	0.3	0.05	Fig. 3(c)
Small-gap Majorana	Ramsey x pulse	12	12	0.5	0	0.016	3	0	Fig. 3(e)
	Ramsey z pulse	14	12	0	0	0.016	3	0	
Large-gap Majorana	Ramsey x pulse	38	38	0.5	0	0.05	0.3	0	Fig. 3(f)
	Ramsey z pulse	40	38	0	0	0.05	0.3	0	

Appendix IV: Quantum capacitance measurement of a Majorana qubit

In this section, we show that quantum capacitance measurement is capable of reading out $|ee\rangle$ and $|oo\rangle$ in a Majorana qubit. We first review the calculations for a single Kitaev chain before generalizing it to a Majorana qubit composed of double Kitaev chains. The zero-temperature quantum capacitance of a state is defined as

$$C_q = -\frac{\partial^2 E}{\partial V_g^2}, \quad (\text{S-1})$$

where E is the eigenenergy of the state, and V_g is the gate voltage. The Hamiltonian of a minimal Kitaev chain can be decomposed into even- and odd-parity sectors due to fermi parity conservation. The even-parity Hamiltonian is

$$H_{\text{even}} = \begin{pmatrix} |00\rangle \\ |11\rangle \end{pmatrix}^T \begin{pmatrix} 0 & \Delta \\ \Delta & \mu_{L1} + \mu_{L2} \end{pmatrix} \begin{pmatrix} \langle 00| \\ \langle 11| \end{pmatrix}, \quad (\text{S-2})$$

where $\mu_{1,2}$ are the onsite energies of the two dots and t, Δ are the normal and Andreev couplings. The ground state energy E_e of $|e\rangle$ is

$$E_e = \frac{\mu_{L1} + \mu_{L2}}{2} - \sqrt{\Delta^2 + \left(\frac{\mu_{L1} + \mu_{L2}}{2}\right)^2}. \quad (\text{S-3})$$

On the other hand, the derivative with respect to gate voltage is

$$\frac{\partial}{\partial V_g} = \alpha_1 \frac{\partial}{\partial \mu_{L1}} + \alpha_2 \frac{\partial}{\partial \mu_{L2}} \approx \alpha \left(\frac{\partial}{\partial \mu_{L1}} + \frac{\partial}{\partial \mu_{L2}} \right), \quad (\text{S-4})$$

where $\alpha_i \equiv d\mu_i/dV_g$ is the lever arm, and here we assume that all dots share a similar value of lever arm α . Therefore, it is straightforward to obtain the quantum capacitance of the even-parity ground state as below

$$C_q^e = -\frac{\partial^2 E_e}{\partial V_g^2} = \frac{\alpha^2}{\sqrt{\Delta^2 + \left(\frac{\mu_{L1} + \mu_{L2}}{2}\right)^2}} - \frac{\alpha^2 (\mu_{L1} + \mu_{L2})^2}{4 \left(\Delta^2 + \left(\frac{\mu_{L1} + \mu_{L2}}{2}\right)^2\right)^{3/2}}. \quad (\text{S-5})$$

At the sweet spot of $\mu_{L1} = \mu_{L2} = 0$, we have

$$C_q^e = \frac{\alpha^2}{\Delta}. \quad (\text{S-6})$$

On the other hand, the Hamiltonian in the odd-parity sector is

$$H_{\text{odd}} = \begin{pmatrix} |10\rangle \\ |01\rangle \end{pmatrix}^T \begin{pmatrix} \mu_{L1} & t \\ t & \mu_{L2} \end{pmatrix} \begin{pmatrix} \langle 10| \\ \langle 01| \end{pmatrix}, \quad (\text{S-7})$$

with ground-state energy being

$$E_o = \frac{\mu_{L1} + \mu_{L2}}{2} - \sqrt{t^2 + \left(\frac{\mu_{L1} - \mu_{L2}}{2}\right)^2}. \quad (\text{S-8})$$

The corresponding quantum capacitance is

$$C_q^o = 0, \quad (\text{S-9})$$

due to the opposite signs of coefficients in front of μ_{L1} and μ_{L2} in the term of $\left(\frac{\mu_{L1} - \mu_{L2}}{2}\right)^2$.

We now generalize our calculations to the quantum capacitance of the double Kitaev chain system. The eigenenergies of the ground states are simply the sum of the left and right chains, i.e.,

$$E_{ab} = E_{aL}(\mu_{L1}, \mu_{L2}) + E_{bR}(\mu_{R1}, \mu_{R2}). \quad (\text{S-10})$$

where a, b denotes the parity e, o . We note that the μ dependence of E is separable between the left and right chains, which indicates that $\partial/\partial V_g \rightarrow \alpha \left(\frac{\partial}{\partial \mu_{L1}} + \frac{\partial}{\partial \mu_{L2}}\right)$ for the left chain energy, while $\partial/\partial V_g \rightarrow \alpha \left(\frac{\partial}{\partial \mu_{R1}} + \frac{\partial}{\partial \mu_{R2}}\right)$ for the right one. Therefore, we have

$$C_q^{ab} = -\frac{\partial^2 E_{ab}}{\partial V_g^2} = -\frac{\partial^2 E_{aL}}{\partial V_g^2} - \frac{\partial^2 E_{bR}}{\partial V_g^2} = C_{qL}^a + C_{qR}^b, \quad (\text{S-11})$$

that is, the quantum capacitance of the state in the whole system is a sum of the value in each chain separately. We therefore have

$$\begin{aligned} C_q^{ee} &= \frac{\alpha^2}{\Delta_L} + \frac{\alpha^2}{\Delta_R}, \\ C_q^{oo} &= 0, \\ C_q^{eo} &= \frac{\alpha^2}{\Delta_L}, \\ C_q^{oe} &= \frac{\alpha^2}{\Delta_R}. \end{aligned} \quad (\text{S-12})$$

Therefore, one can distinguish between $|ee\rangle$ and $|oo\rangle$ states using quantum capacitance measurement. Furthermore, the values of C_q for $|eo\rangle$ and $|oe\rangle$ are generally very different from the qubit states. Thus our method also provides a possible way to investigate the quasiparticle poisoning effect by analyzing the readout results of $|eo\rangle$ and $|oe\rangle$.